Full-sized Pore Structure and Fractal Characteristics of Marine-Continental Transitional Shale: A Case Study in Qinshui Basin, North China

Liangliang YIN[1,2], Shaobin GUO [1,2,*]

[1] *School of Energy resources, China University of Geosciences (Beijing), Beijing 10083, China*
[2] *Key laboratory of strategy evaluation for Shale gas, Ministry of Land and Resources, Beijing 10083, China*

Abstract: Based on 10 shale samples collected from 4 wells in Qinshui Basin, we investigate the full-sized pore structure and fractal characteristics of Marine-Continental transitional shale by performing organic geochemistry, mineralogical composition, Nitrogen gas adsorption (N_2 adsorption) and Nuclear Magnetic Resonance (NMR) measurements and fractal analysis. Results show that the TOC content of the shale samples is relatively high, with an average value of 2.44% (wt.), and the thermal evolution is during the mature-over mature stage. The NMR T_2 spectrum can be used to characterize the full-sized pore structure characteristics of shale. By combining N_2 adsorption pore structure parameters and NMR T_2 spectrums, the surface relaxivity of samples are calculated to be between 1.7877um/s and 5.2272um/s. On this basis, the T_2 spectrums are converted to full-sized pore volume and surface area distribution curves. The statistics show that the pore volume is mainly provided by mesopore, followed by micropore, and the average percentages are 65.04% and 30.83% respectively; the surface area is mainly provided by micropore, followed by mesopore, and the average percentages are 60.8004% and 39.137% respectively; macropore contributes little to pore volume and surface area. The pore structure characteristics of shale have no relationship with TOC, but strong relationships with clay minerals content. NMR fractal dimensions D_{micro} and D_{meso} have strong positive relationships with the N_2 adsorption fractal dimensions D_1 and D_2 respectively, indicating that D_{micro} can be used to characterize the fractal characteristics of pore surface, and D_{meso} can be used to characterize the fractal characteristics of pore structure. The shale surface relaxivity is controlled by multiple factors. The increasing of clay mineral content, pore surface area, pore surface fractal dimension and the decreasing of average pore size, will all lead to the decreasing of shale surface relaxivity.

Keywords: Marine-Continental transitional shale; Nuclear magnetic resonance; Nitrogen adsorption; Full-sized pore structure; Fractal dimensions.

E-mail: guosb58@126.com

1 Introduction

Different from conventional reservoir which has relatively large pores (>1um), shale reservoir has small pores and strong heterogeneity, and it mainly develops nanoscale pores (Zou et al., 2011). With this special pore system, shales have low porosity, permeability and complex pore structure. This will have an important impact on the occurrence state of shale gas (Yu, 2013). Curtis thought that shale gas can be stored in shales in the form of gas adsorbed, free gas or gas dissolved, which were related to the TOC, mineralogical composition and pore structure of shales (Curtis, 2002). It can be seen that identification of the shale pore structure characteristics, including pore volume, specific surface area and pore size distribution, is of great significance for understanding the shale gas adsorption, desorption, diffusion and evaluating the gas content of shale (Chalmers et al., 2012; Loucks et al., 2009; Loucks et al., 2012; Ross and Bustin, 2009).

The previous researchers have done a lot of studies using a variety of methods to characterize the pore structure characteristics of shales. Ar-ion-beam milling and scanning electron microscope were used to qualitatively study the pore types and pore development of shales (Curtis et al., 2012; Fu et al., 2016). Mercury Injection Capillary Pressure (MICP) and N_2 adsorption measurements were performed to quantitatively evaluate the shale pore structure parameters such as the pore volume, specific surface area and pore size distribution (Clarkson et al., 2013; Kuila and Prasad, 2013). In order to study the full-sized pore structure characteristics of shales, Carbon dioxide adsorption (CO_2 adsorption) combined with N_2 adsorption and MICP were conducted to obtain the pore size distribution of micropore (0-2nm), mesopore (2-50nm) and macropore (>50nm) respectively (Jiang et al., 2016). As a rapid and nondestructive new technology, NMR is now being widely used in the

characterization of shale pore structure (Li et al., 2018). According to the NMR relaxation mechanism (Coates et al., 1999), the NMR T_2 spectrum is in correspondence with the pore diameter. Through specific mathematical methods, the NMR T_2 spectrums can be converted to the corresponding pore size distribution curves (Gong et al., 2016), enabling the comprehensive analyses of full-sized pore structure characteristics of shales.

The fractal theory provides a new way to describe the pore structure characteristics of porous media. The fractal dimension can serve to quantitatively characterize the complexity of pore structure (Zhang and Weller, 2014). When studying the pore fractal dimension of porous media (Cai et al., 2015), Cai believed that for two-dimensional space, the pore fractal dimension is between 0 and 2; for three-dimensional space, the pore fractal dimension is between 0 and 3. Based on the analyses of thin sections, Wang used the box-counting method to calculate the pore fractal dimension of marine shales (Wang et al., 2016); Bernal introduced multiple theoretical models for the calculation of fractal dimension using MICP (Bernal and Bello, 2001). In addition, NMR and N_2 adsorption measurements are often used to study the pore fractal characteristics of coals and shales (Cai et al., 2013; Fu et al., 2017; Yang et al., 2014; Yao et al., 2008).

This paper takes the Marine-Continental transitional shale from Qinshui Basin as the research object to analyze the full-sized pore structure and fractal characteristics of shales. The previous researchers have done a lot of studies about the pore structure characteristics of transitional shales, but most of their work was just based on N_2 adsorption measurements. Due to the restriction of this method, it can not be used to analyze the characteristics of micropore and macropore. Therefore, in order to make up for the insufficiency of N_2 adsorption measurements, this paper uses NMR measurements to analyze the full-sized pore structure characteristics of shales. With the combination of NMR and N_2 adsorption measurements (Saidian and Prasad, 2015; Saidian et al., 2014), the full-sized pore structure characteristics of shale samples are investigated based on the pore size distribution curves converted from NMR T_2 spectrums. At the same time, based on the FHH model and NMR fractal theory (Pfeifer and Avnir, 1983), the pore fractal characteristics and its relationships with pore structure parameters are also discussed. This study expands the application range of NMR T_2 spectrum by applying it to the study of full-sized pore structure and fractal characteristics of transitional shale for the first time, which has yielded important results. Moreover, it also has an important guiding significance for the deep use of NMR experimental data and the study of full-sized pore structure characteristics of shale.

2 Geological Settings

The Qinshui Basin is located in the middle of the North China Platform with a nearly north-south trending synclinoria structure. The basin is surrounded by uplifts, i.e. Wutai Mountain uplift in the north, Zhongtiao Mountain uplift in the south, Taihang Mountain uplift in the east, and Lvliang uplift and Huo Mountain bulge in the west (Fig. 1). Before late Paleozoic, the internal structure of the entire North China Platform was relatively stable. As part of the North China Platform, the Qinshui Basin was in the stage of tectonic stability. From late Paleozoic to late Mesozoic, affected by the Indosinian movement, the Qinshui Basin began to take form. Under the influence of the Yanshanian movement, the Lvliang Mountain uplifted to form a mountain, and the Qinshui Basin was subject to uplift and erosion under intense squeezing stress to form an initial shape of synclinoria structure. Since Cenozoic, under the influence of the Himalayan movement, the Qinshui Basin experienced multiple stages of tectonic extension and compression and finally formed the present tectonic pattern (Liang et al., 2016). Under the control of regional tectonic evolution, the Qinshui Basin was in the stage of Marine-Continental transitional environment in the Late Carboniferous-Early Permian, and was dominated by delta, tidal flat, and carbonate platform deposits (Liang et al., 2014). The general stratigraphic column of lower Permian is shown in Fig. 1 with the Taiyuan Formation, Shanxi Formation, and Xiashihezi Formation from bottom to top. The lower Permian in Qinshui Basin develops multiple sets of Marine-Continental transitional shales. Affected by coal seams, the shales have generally high organic matter content, high thermal maturity, and previous studies have shown that the shale gas resource in Qinshui Basin is 0.65 trillion cubic meters. At present, Marine-Continental transitional shale gas has become a key field for the exploration of shale gas (Zhang et al., 2017; Xi et al., 2017). Though Qinshui Basin has abundant shale gas resource, there has not been a full and comprehensive discussion on the petrology, geochemistry, full-sized pore structure and fractal characteristics of the shale reservoir in this area and their relationships with each other. For the purpose of these issues, this study is designed to thoroughly identify the pore structure characteristics of Marine-Continental transitional shale in Qinshui Basin.

3 Samples and Methods

3.1 Sampling and experiments

The 10 shale samples were collected from 4 wells of the lower Permian in Qinshui Basin (Fig. 1), including 7 samples for the Shanxi Formation and 3 samples for the Taiyuan Formation. The sample number and depth of samples are shown in Table 1. The total organic carbon (TOC) of all samples were measured by the carbon-sulfur analyzer Leco according to the Chinese national standard GB/T 19145-2003. The vitrinite reflectance (henceforth referred as Ro) was measured at an ambient temperature of 22°C and a magnification of

125 times by applying microphotometer MPV-SP according to the petroleum and natural gas industry standard SY/T 5124-1995. The mineralogical composition of samples was analyzed by X-ray diffractometer (XRD) D8 DISCOVER through X-Ray Diffraction (XRD) according to the oil and gas industry standard SY/T 5163-2010. The results are shown in Table 1.

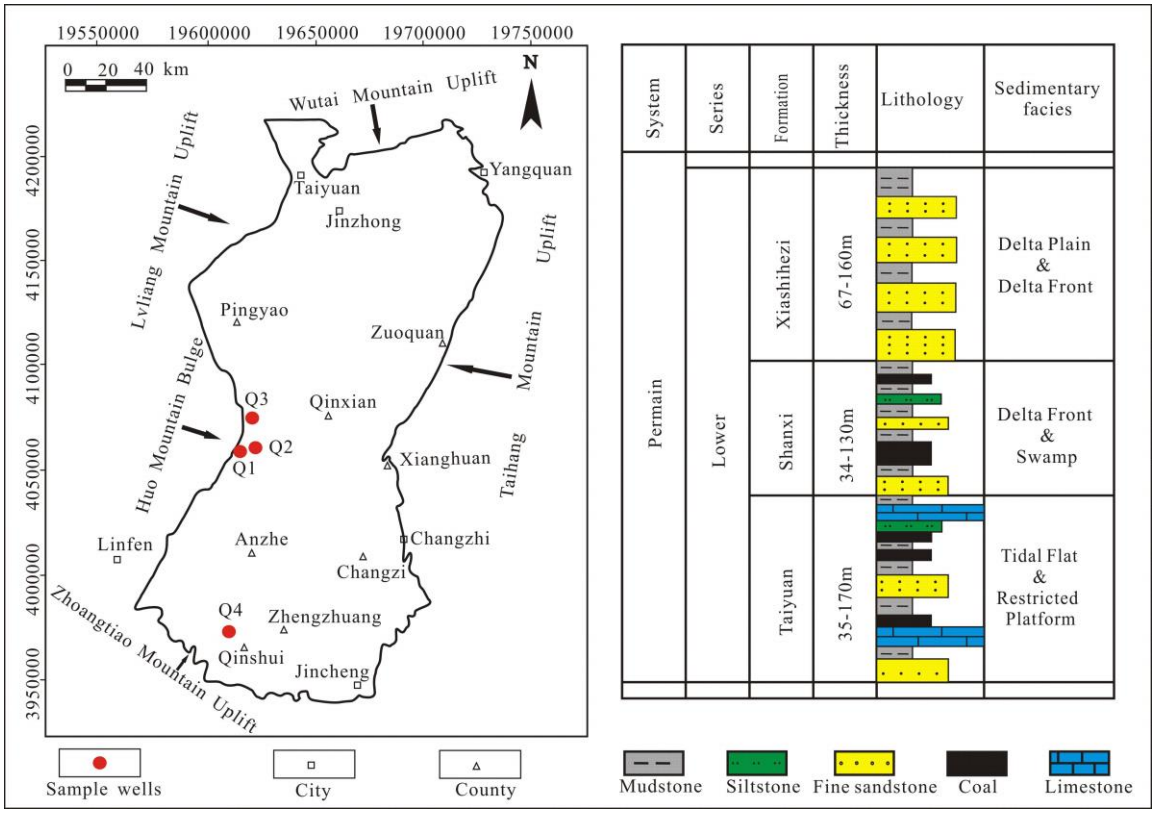

Fig. 1. Location of Qinshui basin (left) and general stratigraphic column of lower Permian in Qinshui Basin (right) (modified from (Liang et al., 2016)).

3.2 N_2 adsorption

According to the national standard GB/T 19587-2004, N_2 adsorption measurements were conducted to obtain the adsorption-desorption isotherms by Quadasorb SI at a temperature of 77K to analyze the pore structure characteristics of shale samples. The specific surface area (henceforth referred as surface area) is calculated according to the Brunauere-Emmete-Teller (BET) model with the relative pressure (P/P0) at the range of 0.05-0.35 (Brunauer et al., 1938). The total pore volume (henceforth referred as pore volume) is determined by the total amount of N_2 adsorbed and the average pore size is calculated according to the method provided in (Quantachrome, 2008). Pore size distribution can be obtained through various computational models, such as DR model and HK model for micropore (Horváth and Kawazoe, 1983; Rand, 1976), and Barrett-Joyner-Halenda (BJH) model and DH model for mesopore (Barrett et al., 1951; Dollimore and Heal, 1964). All of these models are applicable under the premise that the pores are either slit-shaped or cylindrical. Therefore, these models are subject to the premise and the pore size range, and cannot get the pore size distribution of micropore and mesopore at the same time (Yang et al., 2006). Therefore, this study calculates the pore size distribution of shale samples according to the Density Functional Theory (DFT) (Ravikovitch and Neimark, 2006). This theory is applicable to the full isotherms range and can be used to more accurately analyze the pore size distribution of micropore and mesopore. For detailed process, see (Labani et al., 2013).

3.3 Nuclear magnetic resonance (NMR)

Low field NMR measurements were performed using the RecCore-04 instrument according to the petroleum and natural gas industry standard SY/T 6490-2000. For details, see (Yao et al., 2010). Before the measurement, all samples shall first be made into dry samples according to the petroleum and natural gas industry standard SY/T 5336-2006 and then made into fully brine-saturated samples. After the measurements of saturate samples, NMR measurements were performed at an irreducible water condition, where samples were centrifuged under a centrifugal pressure of 400psi. The water salinity, echo spacing, waiting time, number of echoes and number of scans were 40000ppm, 0.3ms, 6s, 2048 and 128 respectively.

Fluids in rock pores have three transverse relaxation mechanisms, i.e. Bulk relaxation time (T_{2B}), Surface relaxation time (T_{2S}), and Diffusion relaxation time (T_{2D}), which can be expressed as the following equation (Coates et al., 1999):

$$\frac{1}{T_2} = \frac{1}{T_{2B}} + \frac{1}{T_{2S}} + \frac{1}{T_{2D}} \quad (1)$$

Where T_2 is the transverse relaxation time of pore fluid. In general, in comparison to the surface relaxation time, the bulk relaxation time and the diffusion time are negligible, so equation (1) (henceforth referred as Eq. (1)) can be transferred to another equation related to the pore diameter, as shown in the following equation:

$$\frac{1}{T_2} = \frac{1}{T_{2S}} = \rho_2 \times \frac{S}{V} = \rho_2 \times \frac{Fs}{R} \quad (2)$$

Where ρ_2 is surface relaxivity which is related to lithology, pore surface and cement (Yan and Liu, 2016), S is the surface area of sample and V is the pore volume of sample (both can be derived from the N_2 adsorption results). R is the pore radius, and Fs is the pore geometry morphologic factor, with Fs=1, 2 or 3 for slit-shaped, cylindrical and spherical pores, respectively (Chu et al., 2007).

From Eq. (2), it can be seen that assuming ρ_2 is a constant, the pore radius R and the transverse relaxation time T_2 values have a one-to-one correspondence, that is, the T_2 time distribution can reflect the pore size distribution of shale samples. Smaller pores correspond to shorter relaxation time, while larger pores correspond to longer relaxation time (Yao et al., 2010). Since the T_2 spectrum is a superposition of the relaxation time of pore system with different pore sizes (Chu et al., 2007; Coates et al., 1999), for the i-th pore system with a surface area of Si and a pore volume of Vi, the transverse relaxation time T_{2i} can be expressed as following:

$$\frac{1}{T_{2i}} = \rho_2 \times \frac{S_i}{V_i} \quad (3)$$

The Eq. (3) shows that the T_{2i} value is in correspondence with the Si/Vi of the i-th pore system. The Eq. (3) can be transferred into the following equation:

$$S_i = \frac{V_i}{\rho_2 \times T_{2i}} \quad (4)$$

After validating the NMR by conventional laboratory porosity measurements (Coates et al., 1999; STRALEY et al., 1997), the pore volume of the i-th pore system can be obtained based on the relative and total magnitude of T_{2i} value and the total porosity measured in the laboratory, and then the pore surface area of i-th pore system can also be obtained based on Eq. (4).

3.4 Fractal theory

There are many models for calculating fractal dimensions based on gas adsorption measurements (Yao et al., 2008). This study used the N_2 adsorption isotherm to calculate the pore fractal dimensions of shale samples based on the FHH model (Pfeifer and Avnir, 1983), which is shown as following:

$$\ln V = k \times \ln\left(\ln\left(\frac{P_0}{P}\right)\right) + C \quad (5)$$

Where V is the gas adsorption amount when the equilibrium pressure is P, and P0 is the saturated pressure of N_2, k is related to the pore fractal dimension D, C is a constant.

The fractal geometry theory was also introduced into the NMR field (Zhang and Weller, 2014). The calculation process is as following:

$$Sv = \frac{T_2^{3-D} - T_{2min}^{3-D}}{T_{2max}^{3-D} - T_{2max}^{3-D}} \quad (6)$$

Where V is the percentage of cumulative pore volume in total pore volume when transverse relaxation time is less than T_2. T_{2min} is the minimum transverse relaxation time, while T_{2max} is the maximum transverse relaxation time, and D is the fractal dimension of pores. When $T_2 >> T_{2min}$, the following equation can be derived from Eq. (6):

$$Sv = \frac{T_2^{3-D}}{T_{2max}^{3-D}} \quad (7)$$

Taking the logarithm to both sides of Eq. (7) results in Eq. (8). For the detailed derivation process, see (Zhang and Weller, 2014).

$$\lg Sv = (3 - D) \times \lg T_2 + (D - 3) \times \lg T_{2max} \quad (8)$$

The following can be obtained from Eq. (2):

$$T_2 = \frac{R}{\rho_2 \times Fs} = \frac{W}{2 \times \rho_2 \times Fs} \quad (9)$$

Where W is the pore diameter, W=2R, ρ_2 is the surface relaxivity, Fs is the pore geometry morphologic factor. ρ_2 and Fs are both constants. Substituting Eq. (9) into Eq. (7) yields the following equation:

$$Sv = \frac{W^{3-D}}{W_{max}^{3-D}} \tag{10}$$

Taking the logarithm to both sides of Eq. (10) results in the following equation:

$$lgSv = (3 - D) \times lgW + (D - 3) \times lgW_{max} \tag{11}$$

Where D is the fractal dimension of the pores, Sv is the percentage of cumulative pore volume in total pore volume when the pore diameter is smaller than W; W_{max} is the maximum pore diameter, and $W>>W_{min}$ is required. From Eq. (11), it can be seen that the fractal characteristics of pores can be studied on the basis of the conversion of the T_2 spectrum into pore size distribution curve.

Table 1 XRD results and geochemical parameters of the lower Permian shale samples

Sample No	Depth (m)	Formation	Ro	TOC (wt. %)	Mineral composition (wt. %)			Clay composition (wt. %)			
					Clay	Q/F	Others	Kaolinite	Chlorite	Illite	I/S
Q1-1	88.15	P_1s	1.74	1.36	56.89	43.11	0.00	18.79	9.49	20.82	50.90
Q1-2	125.95	P_1s	1.51	3.42	57.67	39.95	2.38	19.04	8.48	23.38	49.10
Q1-3	269.78	P_1s	1.76	1.87	52.91	39.17	7.92	31.12	13.86	26.22	28.79
Q2-1	556.68	P_1s	2.14	1.21	50.01	48.13	1.86	23.91	14.39	23.64	38.06
Q2-2	563.93	P_1s	1.96	3.78	58.74	41.26	0.00	33.94	14.90	16.70	34.45
Q2-3	584.33	P_1t	2.22	0.92	53.70	44.19	2.12	25.97	9.77	19.27	44.99
Q3-1	574.59	P_1s	1.93	0.91	59.79	39.43	0.78	27.01	12.06	17.24	43.69
Q3-2	636.16	P_1t	1.95	7.21	61.64	38.36	0.00	43.18	11.07	12.85	32.90
Q3-3	712.66	P_1t	2.10	2.59	59.79	38.91	1.31	42.93	7.21	18.76	31.10
Q4	901.44	P_1s	2.03	1.12	62.97	35.98	1.05	23.91	9.27	23.13	43.69
Average			1.93	2.44	57.41	40.85	1.74	28.98	11.05	20.20	39.77

Q/F: Quartz and Feldspar; I/S: Illite-Smectite layer-mixed mineral; Others: containing pyrite and carbonates.

4 Results

4.1 Geochemical characteristics and mineralogical composition

Table 2 N_2 adsorption results

Sample No.	Surface area (m2/g)	Pore volume (cm3/g)	Average pore size (nm)	Hysteresis loop size
Q1-1	4.145	0.01030	9.94	0.53
Q1-2	4.423	0.00881	7.97	0.59
Q1-3	4.903	0.00447	3.65	0.16
Q2-1	3.559	0.00746	8.38	0.65
Q2-2	2.840	0.00491	6.91	0.37
Q2-3	3.633	0.00939	10.34	0.65
Q3-1	6.439	0.01142	7.09	0.84
Q3-2	3.936	0.00602	6.12	0.32
Q3-3	5.192	0.00479	3.69	0.16
Q4	3.493	0.00678	7.77	0.46

Surface area= Specific Surface area; Pore volume= Total pore volume; Hysteresis loop size: integral of desorption volume minus adsorption volume indicating the relative size of hysteresis loop.

The TOC, Ro and mineralogical composition of the 10 samples are shown in Table 1. The TOC of samples varies from 0.91% (wt.) to 7.21% (wt.), and different samples have significantly different TOC. As shown in Table 1, the lower Permian shale in Qinshui Basin has relatively high TOC, with an average value of 2.44% (wt.). The Ro varies from 1.51% to 2.22% with an average value of 1.93%, indicating that the organic matter has a high thermal maturity, during the mature-over mature stage, and mainly generates dry gas. XRD results

show that the mineralogical composition of samples is mainly clay minerals ranging from 50.51% (wt.) to 62.97% (wt.) with an average content of 57.41% (wt.), followed by quartz and feldspar ranging from 35.98% (wt.) to 48.13% (wt.) with an average content of 40.85% (wt.), and also some other minerals, including pyrite and carbonates with an average content of 1.74% (wt.). The clay minerals are mainly I/S and kaolinite with an average relative content of 39.77% (wt.) and 28.89% (wt.) respectively, followed by illite and chlorite with an average relative content of 20.2% (wt.) and 11.05% (wt.) respectively.

4.2 N2 adsorption results

The N_2 adsorption results are shown in Table 2. The surface area is between 2.84m2/g and 6.349m2/g with an average value of 4.256m2/g; the pore volume is between 4.47 (×10-3 cm3/g) and 11.42 (×10-3 cm3/g) with an average value of 7.44 (×10-3 cm3/g); the average pore size is between 3.64nm and 10.34nm with an average value of 7.19nm. The hysteresis loop size is between 0.16 and 0.84 with an average value of 0.47. There is no unit for this number which is only used to indicate the relative size of the hysteresis loop for different samples. From Table 2, it can be seen that the pore structure parameters of the 10 samples are quite different. This is related to the difference of TOC, mineralogical composition and pore structure. The relationships between them will be further discussed in the following

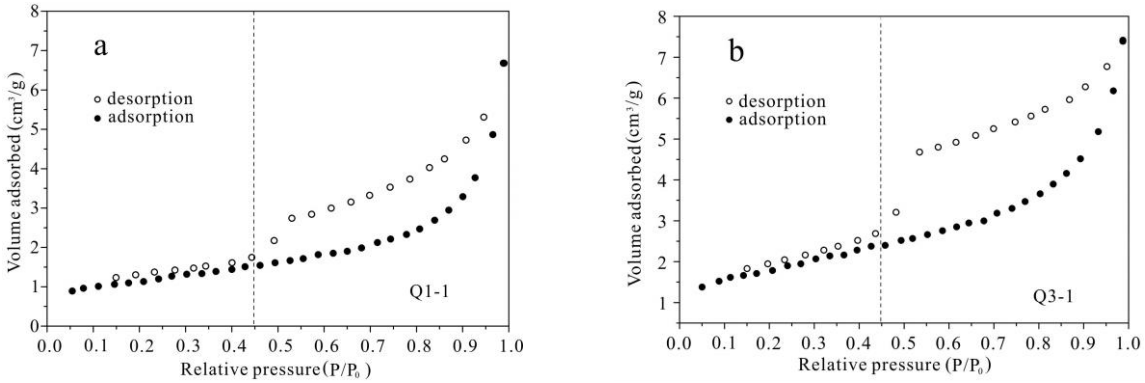

Fig. 2. N_2 adsorption-desorption isotherms of two shale samples.

According to the interpretation process of adsorption isotherm proposed by (Sing et al., 1985), the isotherms type should be first identified; then the adsorption mechanism should be identified to be monolayer-multilayer adsorption, capillary condensation or micropore filling; the last to be identified is the hysteresis loop type. These factors are all related to pore types and pore structure (Kuila and Prasad, 2013; Labani et al., 2013; Xiong et al., 2017).

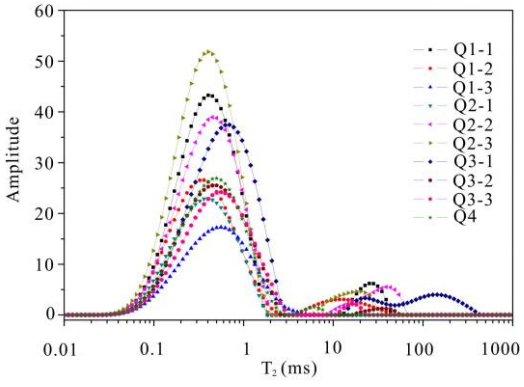

Fig. 3. T_2 spectrums of all shale samples.

According to IUPAC's classification of adsorption isotherms (Sing et al., 1985), the adsorption isotherms of both samples in Fig. 2 are Type IV isotherm, and the adsorption process can be divided into two stages. At the stage of low relative pressure (0<P/P0<0.45), the adsorption branch and the desorption branch of the isotherms superpose nearly, indicating that this stage is monolayer-multilayer adsorption; at the stage of high relative pressure (0.45<P/P0<1), the desorption branch of the isotherm is separated from the adsorption branch, indicating that this stage is capillary condensation. The most obvious feature of Type IV isotherm is a distinct hysteresis loop which is associated with capillary condensation taking place in mesopore (Sing et al., 1985).

According to IUPAC's classification of hysteresis loops, the hysteresis loops of both samples in Fig. 2 are Type H3 hysteresis loop. The characteristic feature of Type H3 hysteresis loop is its adsorption at the range of high P/P0 showing no limiting uptake, which is identical with the characteristics of the hysteresis loop in Fig. 2. According to IUPAC's description of the relationships between the hysteresis loop and the pore shape, the Type H3 hysteresis loop denotes slit-shaped pores which are associated with plate-like particles related to the aggregates of clay minerals (Yang et al., 2017). Only the adsorption-desorption isotherms of two samples are shown here and the other eight samples are the same as those of the two, which will not be repeated. Based on the above analysis, the mesopores of all samples in the research are well developed and the pore shape mainly slit-shaped.

4.3 Surface relaxivity and full-sized pore structure from NMR

4.3.1 Surface relaxivity calculation

Regarding the calculation of the surface relaxivity, many previous studies have been done (Benavides et al., 2017; Fleury, 2007). It is believed that the surface relaxivity is not only subject to lithology, but also related to pore surface and pore size. Even for the same sample, its surface relaxivity also varies with pore size. However, measuring the surface relaxivity for every individual pore is not practical and a fixed surface relaxivity of one sample is convenient to study the pore size distribution. The previous methods for calculating the surface relaxivity can be summarized in three types (Saidian and Prasad, 2015): I. According to the pore or throat size distribution characteristics obtained through measurements, such as MICP, N_2 adsorption, or image analysis, the iterative method is used to continuously modify the value of surface relaxivity to match the NMR T_2 spectrum. II. The surface relaxivity is calculated via the surface area obtained through measurements, such as N_2 adsorption or MICP. III. The surface relaxivity is calculated by combining different NMR measurements. As the samples in the research area is shale with small pore size and complex pore structure, Method III is not applicable. A lot of work has been done as to Method I (Gong et al., 2016; Ning et al., 2016), but it is vulnerable to human factors, resulting in large error in calculation results. Therefore, this study uses Method II to calculate the surface relaxivity of shale samples. For the convenience of this study, it is assumed that the surface relaxivity of the same sample is a constant, and the surface relaxivity is calculated by the NMR T_2 spectrum (Fig. 3) and the N_2 adsorption results (Table 2) (Saidian and Prasad, 2015; Saidian et al., 2014).

It can be seen from Eq. (2) that when the surface area (S) and the pore volume (V) are known, to calculate the surface relaxivity ρ_2, the key is to accurately select the T_2 value. This study uses the method proposed in (Saidian and Prasad, 2015), adopting the logarithmic mean of the T_2 spectrum to represent the distribution characteristics of the entire T_2 spectrum, as shown in the following equation:

$$T_{2LM} = \exp^{\left(\frac{\sum \ln(T_{2i}) \times \varphi_i}{\sum \varphi_i}\right)} \tag{12}$$

Where T_{2LM} is the logarithmic mean of T_2 distribution, T_{2i} is the T_2 value corresponding to the i-th pore system, and φ_i is the porosity of the i-th pore system. Substituting Eq. (12) into Eq. (2) yields:

$$\rho_2 = \frac{V}{S \times T_{2LM}} \tag{13}$$

Where S is the surface area and V is the pore volume, which are obtained by N_2 adsorption results. The surface relaxivity of all samples can be calculated according to Eq. (13). The calculated results are shown in Table 3. The surface relaxivity of the 10 samples varies from 1.7877um/s to 5.2772um/s with an average value of 3.7995um/s, which is consistent with the study of (Chu et al., 2007; Saidian and Prasad, 2015).

Table 3 Calculated surface relaxivity using N_2 adsorption

Sample No	S(m2/g)	V(cm3/g)	T_{2LM}(ms)	ρ_2 (um/s)
Q1-1	4.145	0.01030	0.4709	5.2772
Q1-2	4.423	0.00881	0.4558	4.3697
Q1-3	4.903	0.00447	0.4802	1.8986
Q2-1	3.559	0.00746	0.3492	6.0033
Q2-2	2.840	0.00491	0.5501	3.1425
Q2-3	3.633	0.00939	0.4365	5.9207
Q3-1	6.439	0.01142	0.9017	1.9668
Q3-2	3.936	0.00602	0.4730	3.2352
Q3-3	5.192	0.00479	0.5159	1.7877
Q4	3.493	0.00678	0.4419	4.3939

S=Surface area; V=Pore volume.

The relaxation mechanism of rock is mainly controlled by fluid-solid interaction (surface relaxation), and the surface relaxivity can quantitatively quantify the transverse relaxation mechanism. However, when the rock contains paramagnetic minerals, it will interact strongly with the hydrogen nuclei spins in the pore fluid, resulting in enhanced surface relaxation mechanism and larger surface relaxivity. As a result, it is impossible to accurately measure the transverse relaxation time from the pore fluid, and then affect the use of NMR T_2 spectrum to study the pore structure characteristics of rock (Yan and Liu, 2016). Some shale samples in the research area contain paramagnetic mineral pyrite, so it is necessary to analyze its effect on the surface relaxation mechanism. Saidian pointed out that although pyrite had high iron content and magnetic susceptibility, shale was mainly composed of quartz and clay minerals, and the proportion of pyrite was relatively small (Saidian and Prasad, 2015). The little pyrite content (<1 wt.%) does not have much influence on the magnetic sensitivity of the rock, nor does it affect the surface relaxation mechanism and the calculation of the surface relaxivity. Li also showed that when the content of paramagnetic minerals was small, it would not have a significant impact on the NMR porosity (Li et al., 2014). According to the analysis of the mineralogical composition in the research area, the average content of pyrite and carbonates is less than 2.5% (wt.). Besides, by combining the detailed analysis of previous studies on the mineralogical composition of lower Permian shale in Qinshui Basin (Xi et al., 2017), it can be concluded that the pyrite content in the research area is also less than 1% (wt.). In another word, pyrite wouldn't affect the surface relaxation mechanism of samples, which means that the T_2 spectrums obtained by the NMR measurements and the surface relaxation calculated by Eq. (13) are reliable.

4.3.2 Full-sized distribution of pore volume and surface area

According to the analyses of N_2 adsorption isotherms, the hysteresis loop type for all samples is H3 type, which is related to the slit-shaped pores. The mineralogical composition results show that the mineralogical composition of the samples is mainly clay minerals which are characterized by layered structure (Ji et al., 2012). These characteristics can determine that the pore type of the samples in the research area is mainly slit-shaped pore, and then the pore geometry morphological factor in Eq. (2) can be determined, i.e. Fs=1 (section 3.3).

The Eq. (2) can be transferred into the following equation:

$$W = 2R = 2T_2\rho_2 Fs \tag{14}$$

Where W is the pore diameter, and ρ_2 is the surface relaxivity which can be obtained by Eq. (13). T_2 is the transverse relaxation time, and Fs=1.

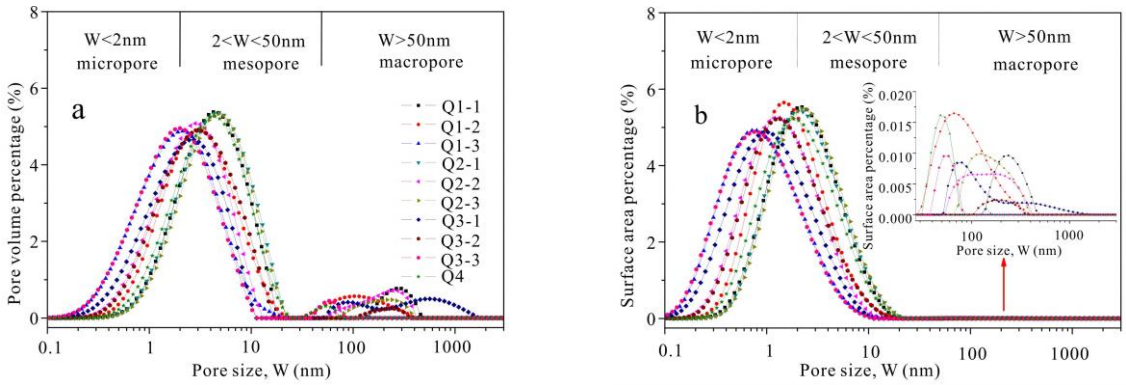

Fig. 4. Full-sized pore volume (a) and surface area (b) distribution obtained from NMR.

Based on Eq. (14), the transverse relaxation time can be converted to the corresponding pore diameter, and through combination with the relative amplitude of the T_2 spectrums (Fig. 3), the pore volume percentages of different pore sizes can be calculated to obtain the full-sized pore volume distribution curves for all samples (Fig. 4a). Based on the full-sized pore volume distribution curves, the full-sized surface area distribution curves (Fig. 4b) can be obtained according to Eq. (14). Here, the vertical axes of the full-sized pore volume and surface area distribution curves refer to the percentage of pore volume and surface area in the total pore volume and total surface area respectively. With no doubt, if the porosity, volume, and density of the samples are known, the true pore volume and surface area of pores can be obtained directly.

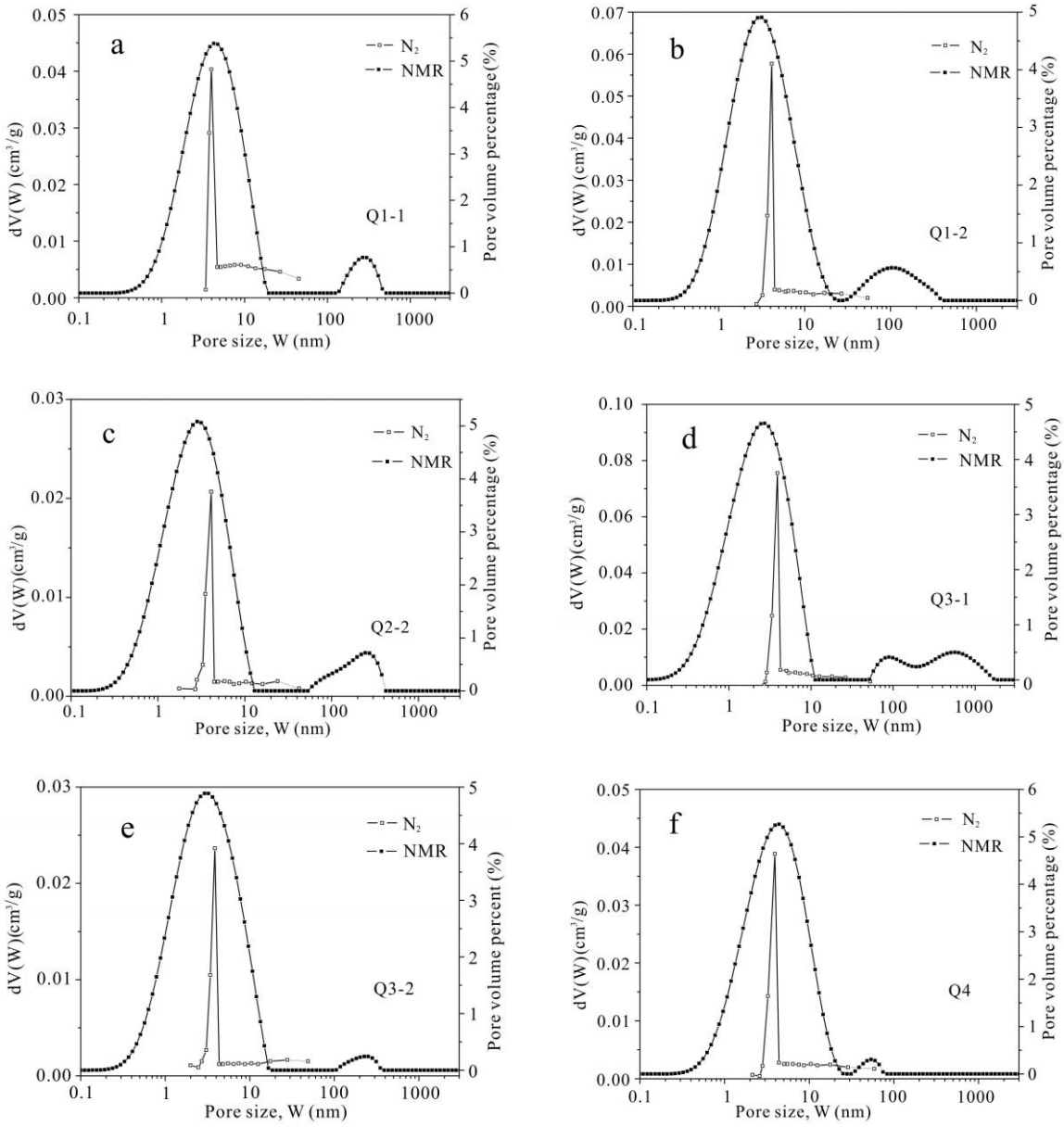

Fig. 5. Comparison of pore size distributions obtained from N_2 adsorption and NMR.

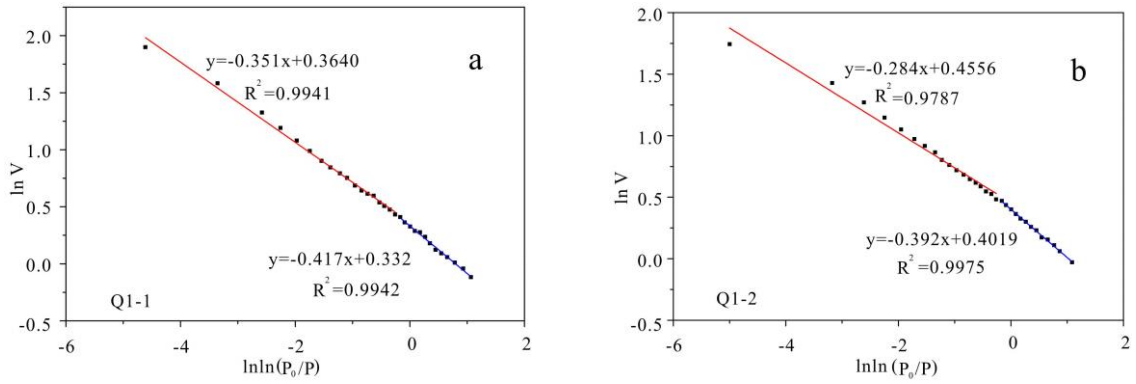

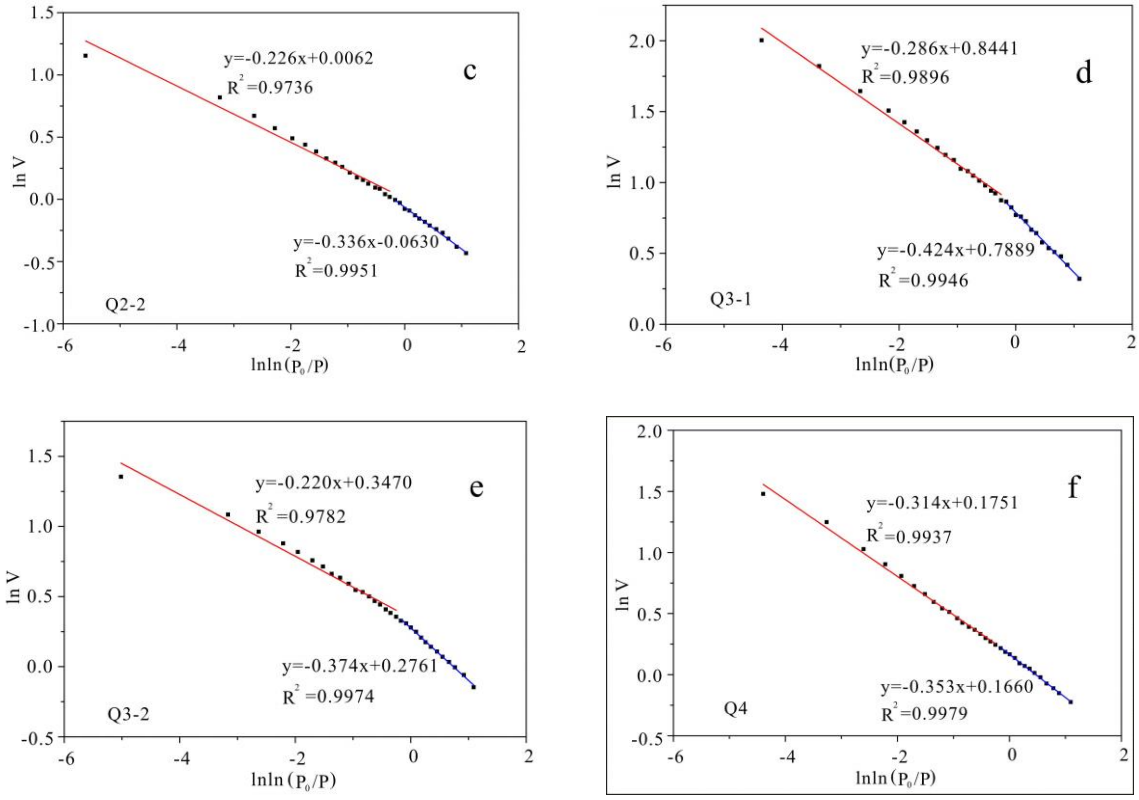

Fig. 6. Plots of ln V vs. lnln (P_0/P) obtained from N_2 adsorption isotherms.

4.4 Fractal dimensions from N2 adsorption and NMR

As the FHH model suggest, the lnV vs ln(P0/P) curve is plotted using the adsorption branch isotherm based on Eq. (5), and the curve is fitted linearly. With this method, linear fitting is performed on the curves plotted for all samples (Fig. 6). There are two distinct linear segments for the six samples at the relative pressure (P/P0) range of 0-0.45 and 0.45-1 respectively, displaying good fitting effect, and the R^2 is greater than 0.95. These phenomena indicate that pores in shale samples have different fractal characteristics at different relative pressure ranges, which are mainly related to the phases during adsorption process (Yao et al., 2008). Previous studies showed that at the relative pressure (P/P0) range of 0-0.45, gas molecules mainly generate monolayer-multilayer adsorption (Yang et al., 2017). The fractal characteristics at this range can be considered as mainly reflecting the complexity of the pore surface. As the fractal dimension gets larger, the pore surface becomes more irregular and rougher. At the relative pressure (P/P0) range of between 0.45-1, gas molecules mainly generate capillary condensation. The fractal characteristics at this range can be considered as mainly reflecting the complexity of the pore structure. Larger fractal dimension represents higher heterogeneity of pore structure.

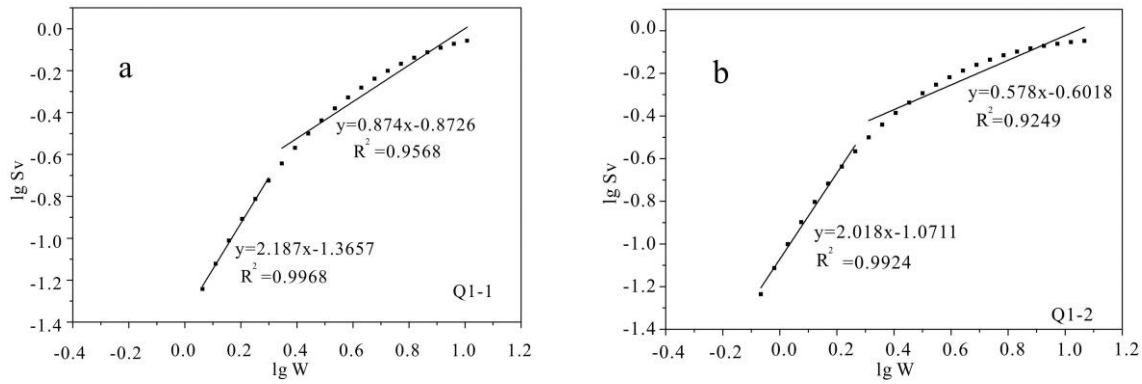

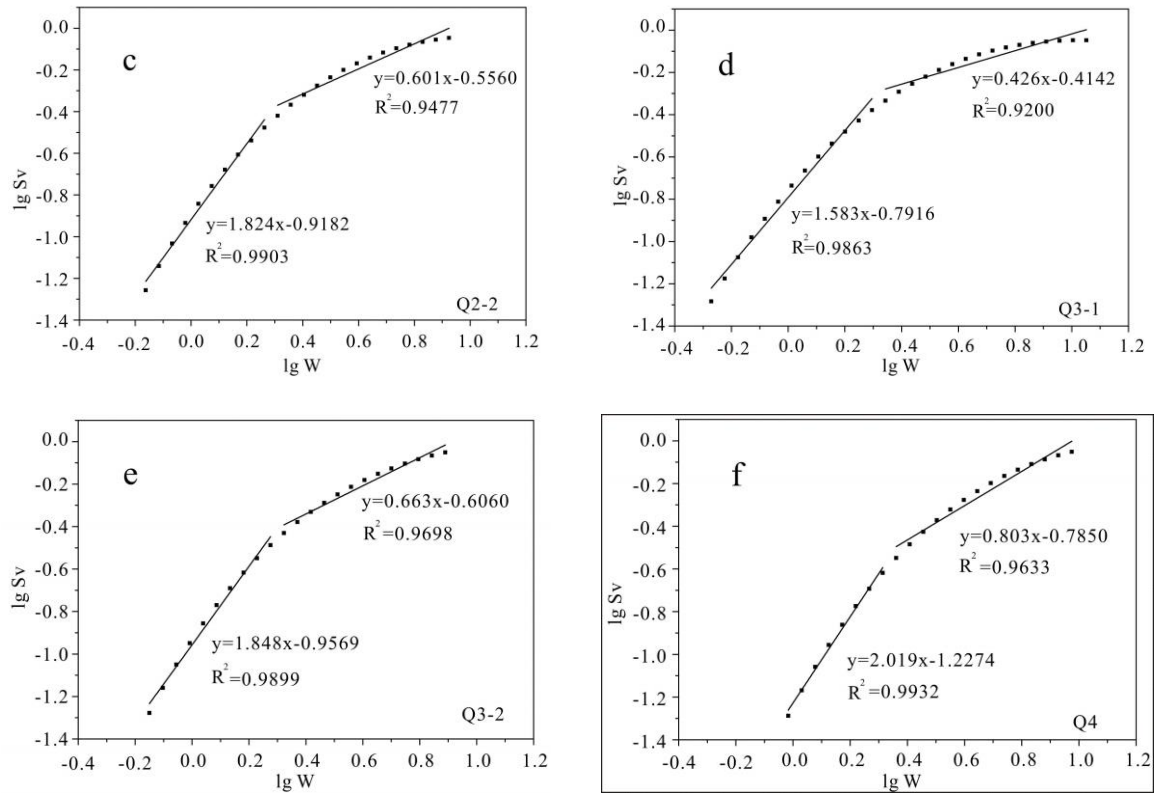

Fig. 7. Plots of lg Sv vs. lg W obtained from NMR.

To calculate the pore fractal dimension according to the linear fitting slope k, there are two different methods: one is D=k+3, and the other is D=3k+3. This study, based on previous analyses (Yang et al., 2014; Yao et al., 2008), uses the first method (D=k+3) to calculate the pore fractal dimension. According to the linearly fitted slopes k_1 ($0<P/P0<0.45$) and k_2 ($0.45<P/P0<1$) at different relative pressure ranges, the corresponding pore fractal dimension D_1 ($D_1=k_1+3$) and D_2 ($D_2=k_2+3$) can be obtained. Table 4 summarizes the slope and R^2 of the linear fitting, and the calculated fractal dimensions for all samples.

The NMR fractal theory conducted by previous studies are all based on a fixed T_2 value (Li et al., 2018; Zhou and Kang, 2016; Zhou et al., 2016), such as T_2=2.5ms or T_2= $T_{2\,cutoff}$. They divided the T_2 spectrum into two segments and specify each segment to represent different pore type to study the pore fractal characteristics. However, due to the variance of surface relaxivity and pore structure to different samples, a fixed T_2 value cannot precisely distinguish different pore types, and the calculated fractal dimension cannot truly represent the fractal characteristics of corresponding pore type.

Table 4 Calculated fractal dimensions from N_2 adsorption isotherms and NMR

Sample No	$0<P/P_0<0.45$			$0.45< P/P_0<1$			$0<W<2nm$			$2<W<50nm$		
	k_1	R^2	D_1	k_2	R^2	D_2	k_3	R^2	D_{micro}	k_4	R^2	D_{meso}
Q1-1	-0.417	0.9942	2.583	-0.351	0.9941	2.649	2.187	0.9968	0.813	0.874	0.9568	2.126
Q1-2	-0.392	0.9975	2.608	-0.284	0.9787	2.716	2.018	0.9924	0.982	0.578	0.9249	2.422
Q1-3	-0.284	0.9902	2.716	-0.122	0.9617	2.878	1.507	0.9794	1.493	0.537	0.9854	2.463
Q2-1	-0.425	0.9946	2.575	-0.316	0.9862	2.684	2.255	0.9974	0.745	0.918	0.9597	2.082
Q2-2	-0.336	0.9951	2.664	-0.226	0.9736	2.774	1.824	0.9903	1.176	0.601	0.9477	2.399
Q2-3	-0.426	0.9926	2.574	-0.341	0.9820	2.659	2.272	0.9988	0.728	0.937	0.9503	2.063
Q3-1	-0.424	0.9946	2.576	-0.286	0.9896	2.714	1.583	0.9863	1.417	0.426	0.9200	2.574
Q3-2	-0.374	0.9974	2.626	-0.220	0.9782	2.780	1.848	0.9899	1.152	0.663	0.9698	2.337
Q3-3	-0.285	0.9917	2.715	-0.101	0.9564	2.899	1.494	0.9837	1.506	0.520	0.9795	2.480
Q4	-0.353	0.9979	2.647	-0.314	0.9937	2.686	2.019	0.9941	0.981	0.803	0.9661	2.197

k_i: fitting slope; R^2: correlation coefficient; D_{micro}: the fractal dimension of micropore; D_{mseo}: the fractal dimension of mesopore.

In order to more truly reflect the fractal characteristics of different pore types, this study firstly obtains the pore size distribution curves converted from the T_2 spectrums, and then calculates the fractal dimensions of different pore types according to the IUPAC's pore size classification standard. In order to make the Eq. (11) true, $W>>W_{min}$ is required. Therefore, before the pore fractal dimension calculation is performed, pretreatments need to be done to the por size distribution curves (Zhang and Weller, 2014). It can be seen from Fig. 4 that the pore size distribution curves obtained from the conversion of T_2 spectrums are quite different, and the macropore are poorly developed compared to micropore and mesopore, with an average pore volume percentage of less than 5%. Based on the above analysis, this study selects the cumulative porosity curves between 5% and 90% for linear fitting to analyze the fractal characteristics of micropore and mesopore. After being plotted based on Eq. (11), the lgSv vs lgW curve is linearly fitted to obtain the slope k. Then the fractal dimension D (D=3-k) can be obtained (Fig. 7). Table 4 summarizes the slope and R^2 of the linear fitting, and the calculated fractal dimension of micropore and mesopore.

5 Discussions

5.1 Full-sized pore structure characteristics

According to the IUPAC's pore classification standard (Sing et al., 1985), pores can be classified into three categories according to the pore size: micropore (<2 nm), mesopore (2-50 nm) and macropore (>50 nm). It can be seen from Fig. 4a that the pore size distribution curves converted from NMR T_2 spectrums have a range of 0.2-2000nm, and the distribution characteristics of micropore, mesopore and macropore can be obtained at the same time. The full-sized pore volume distribution pattern can be classified as unimodal (e.g. Fig. 4a, Q1-3, Q2-1, Q3-3) which only develops micro-mesopore, and bimodal (e.g. Fig. 4a Q1-1, Q1-2, Q2-2, Q2-3, Q3-2, Q4) and trimodal (e.g. Fig. 4a Q3-1), both of which develop micro-, meso-and macropore, with higher percentage of macropore for trimodal. As it can be seen from Table 5, the average pore volume percentage of mesopore is the largest, reaching 65.04%, followed by micropore and macropore, which is 30.83% and 4.13% respectively. The pattern of the full-sized pore surface area distribution curves of all samples is basically unimodal (Fig. 4b). The main modes are mainly between 0.5nm and 5nm, and the contribution of pores larger than 20nm to surface area is almost negligible. As it can be seen from Table 5, the average surface area percentage of micropore is the largest, reaching 60.8004%, followed by mesopore and macropore, which is 39.137% and 0.0626% respectively.

Table 5 The percentage of pore volume and surface area of different pores from NMR

Sample No	Pore volume percentage (%)			Surface area percentage (%)		
	micropore	mesopore	macropore	micropore	mesopore	macropore
Q1-1	18.84	75.36	5.80	46.4799	53.4477	0.0724
Q1-2	27.18	65.34	7.48	59.1990	40.6336	0.1674
Q1-3	53.10	46.90	0.00	82.7000	17.3000	0.0000
Q2-1	16.08	83.87	0.05	41.4277	58.5711	0.0012
Q2-2	33.34	58.75	7.91	66.6242	33.2782	0.0976
Q2-3	13.58	81.16	5.26	37.9173	61.9750	0.1077
Q3-1	41.82	47.67	10.51	77.2640	22.6466	0.0894
Q3-2	32.53	65.65	1.82	65.2937	34.6873	0.0190
Q3-3	51.57	46.83	1.60	81.8585	18.1089	0.0326
Q4	20.27	78.90	0.83	49.2393	50.7218	0.0389
Average	30.83	65.04	4.13	60.8004	39.1370	0.0626

Comparing the pore size distribution curves obtained by NMR and N_2 adsorption measurements (Fig. 5), the main modes of the two methods are basically identical, both between 3-5 nm. In addition to analyze the pore size distribution characteristics of mesopore, NMR can also be used to analyze those of micropore and macropore, while N_2 adsorption is mainly used to analyze the pore size distribution characteristics of mesopore. To characterize the full-sized pore distribution of shale, it is also necessary to combine other measurements such as CO2 adsorption and MICP (Ross and Bustin, 2009; Jiang et al., 2016; Chen et al., 2017; Han et al., 2018; Zuo et al., 2017). Different from gas adsorption and MICP that require the fluid to enter the pore space from the exterior of sample, NMR, as a non-destructive technique, analyzes the pore size distribution including connected and disconnected pores only by measuring the relaxation time (the relaxation time corresponds to the pore size) produced by the fluid-solid interaction in the pores, and then describe full-sized pore structure characteristics of shale samples.

5.2 Relationships between pore structure and TOC, mineralogical composition

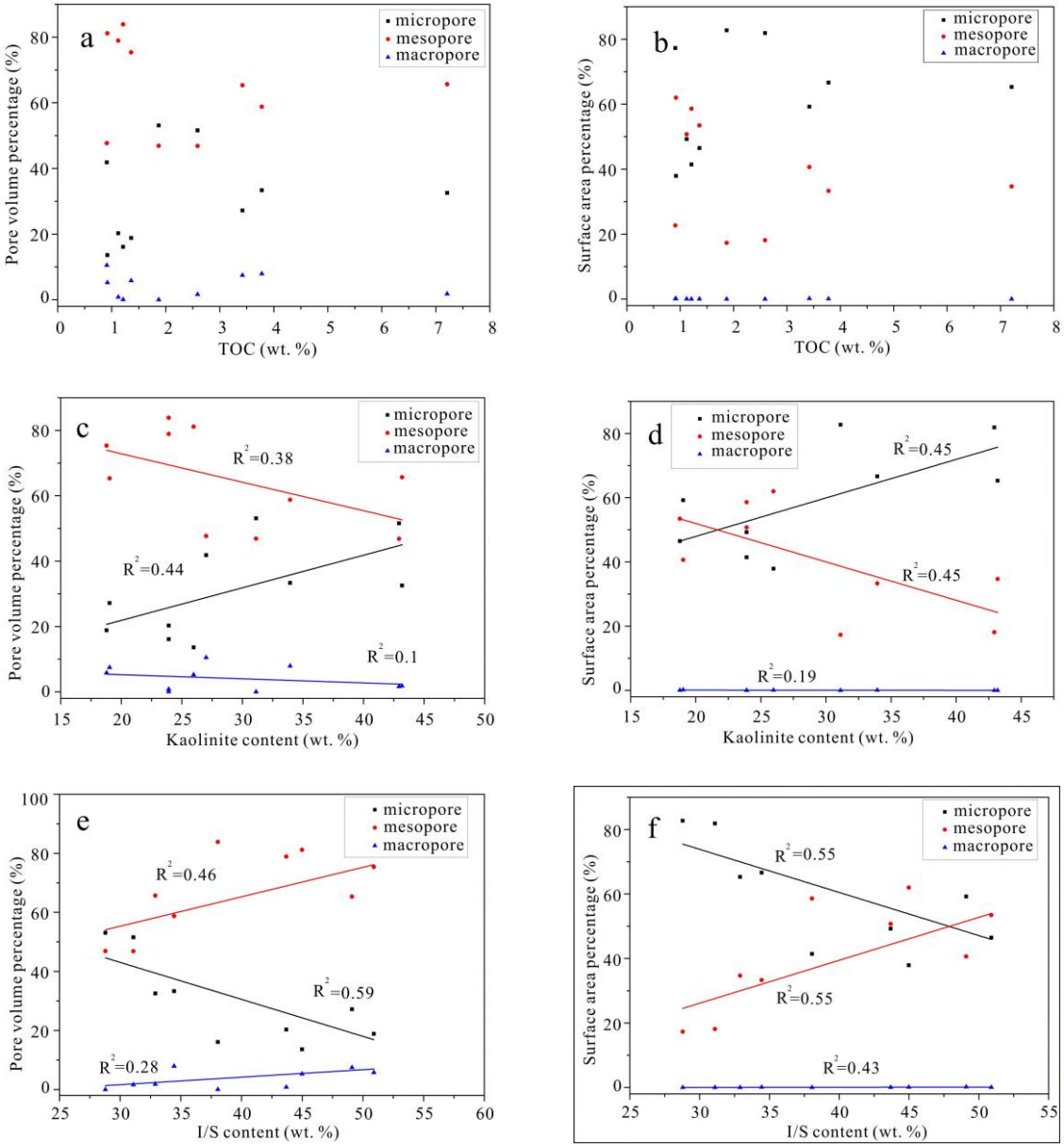

Fig. 8. Relationships between relative pore volume, relative surface area and TOC (a, b), Kaolinite content (c, d), I/S content (e, f).

The relationships of pore volume and surface area of shale samples with TOC and mineralogical composition are shown in Fig. 8. The relative pore volume and surface area of different pore types have no relationships with TOC, or there are light negative relationships (Fig. 8a-b). Through the comparison of Table 1 and Table 5, it can be seen that the relative pore volume and surface area of different pore types have no relationships with brittle minerals content, but strong relationships with clay minerals content (Fig. 8c-f). These characteristics indicate that the pore volume and surface area of shale samples mainly come from clay minerals, while organic matter and brittle minerals have little or no contribution to them. This is consistent with previous researches (Zhang et al., 2017). Due to its special depositional environment, marine shales have a high content of organic matter and develop abundant organic pores (Loucks et al., 2009). Its pore volume and surface area are obviously controlled by TOC (Wang et al., 2016). However, the high thermal maturity and type III kerogen (Xi et al., 2017), which are not conducive to the generation of organic pores (Yang et al., 2017), result in the pore volume and surface area not controlled by TOC for the samples studied in this paper.

Fig. 8c-f shows that the controlling factors of the relative pore volume and surface area of micropore, mesopore and macropore are different. The relative pore volume and surface area of micropore and

mesopore-macropore are mainly controlled by kaolinite (Fig. 8c-d) and I/S content respectively (Fig. 8e-f). These results may be related to the well-developed mesoscale intra-aggregate pores and macroscale inter-aggregate pores in I/S, and well-developed microscale intergranular pores in kaolinite (Kuila and Prasad, 2013; Ji et al., 2012). It should be pointed out that clay minerals tend to have abundant pore space. The negative relationships between the relative pore volume, surface area of mesopore, micropore and kaolinite content (Fig. 8c-d), I/S content (Fig. 8e-f) respectively are not caused by kaolinite or I/S itself, but caused passively by the negative relationship between kaolinite content and I/S content (Table 1). Since the chlorite and illite have few pores, they do not contribute much to the pore structure parameters and their relationships are not discussed here.

5.3 Relationships between fractal dimensions and pore structure

The relationships between fractal dimension and pore structure parameters are shown in Fig. 9. The relative pore volume and relative specific surface area of micropore both have strong positive relationship with NMR fractal dimension D_{micro}, and the R^2 is 0.96 and 0.97 respectively (Fig. 9a). In contrast, the relative pore volume and relative surface area of mesopore both have strong negative relationship with NMR fractal dimension D_{meso}, and the R^2 is 0.88 and 0.87 respectively (Fig. 9b). This shows that with the increasing of relative pore volume and relative surface area, the variation of fractal characteristics of micropore and mesopore are divergent. As the micropore percentage gets higher, the corresponding pore structure becomes more complex, and the pore surface gets rougher and more irregular; as the mesopore percentage gets higher, the corresponding pore structure becomes more complex, and the pore surface gets smoother and more regular. The BET surface area has a light positive relationship with N_2 fractal dimension D_1 (Fig. 9c), showing that as the pore surface area gets larger, the pore surface will become rougher and more irregular. The pore volume has a strong negative relationship with the N_2 fractal dimension D_2 (Fig. 9d), indicating that as the pore volume gets larger, the complexity of pore structure becomes lower.

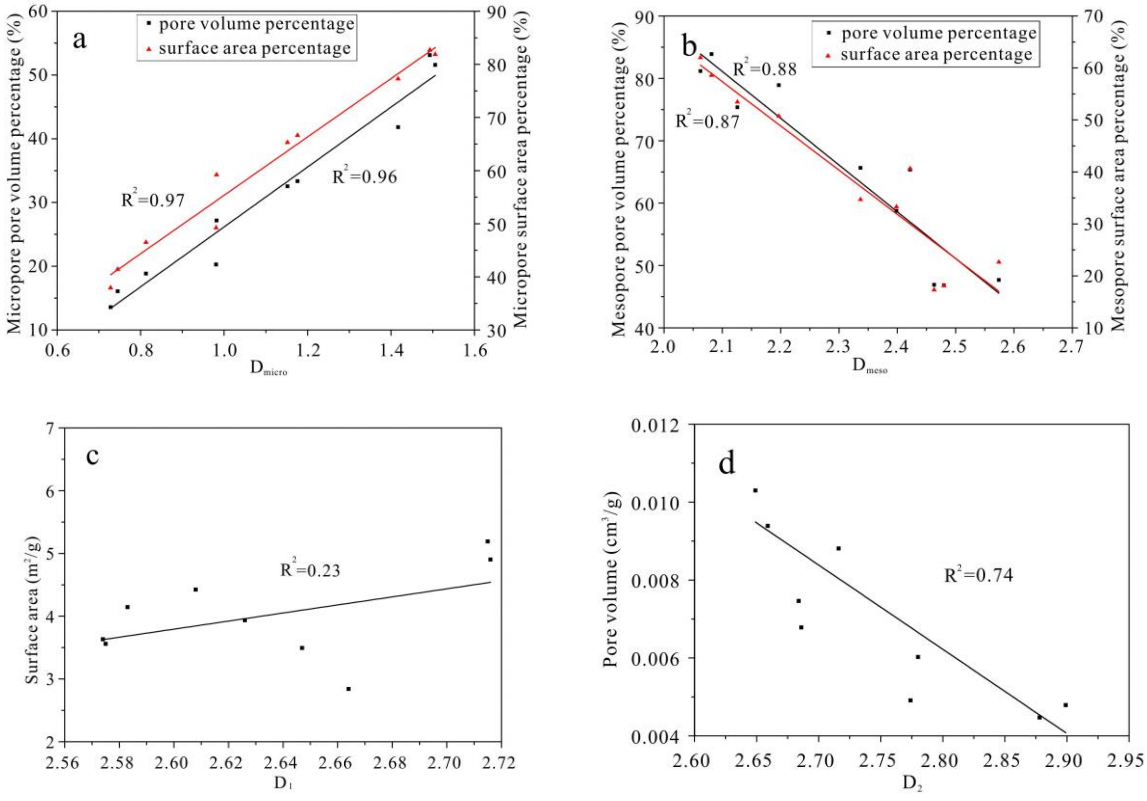

Fig. 9. Relationships between NMR and N_2 fractal dimensions and pore sturcture parameters.

5.4 Comparison of fractal dimensions from N2 adsorption and NMR

The relationships between the NMR fractal dimension and the N_2 adsorption fractal dimension are shown in Fig. 10a-b. There are strong positive relationships between D_{micro} and D_1, D_{meso} and D_2, and the R^2 is 0.93 and 0.74 respectively. This proves that although the principles of NMR and N_2 adsorption measurements are not the same, and the fractal dimension calculation methods are also different, their fractal dimensions have a strong consistency. Pyun thought that the fractal dimensions of porous media include pore structure fractal dimension and pore surface fractal dimension (Pyun and Rhee, 2004). Previous studies all believed that the fractal

dimension D_1 represents the fractal dimension of the pore surface (Fu et al., 2017; Yang et al., 2014; Yao et al., 2008). As the fractal dimension D_1 gets larger, the pore surface becomes rougher and more irregular; The fractal dimension D_2 represents the fractal dimension of the pore structure. As the fractal dimension D_2 gets larger, the pore structure becomes more irregular. In this study, the fractal dimensions of the micropore (D_{micro}) and mesopore (D_{meso}) are calculated separately based on the conversion of T_2 spectrums to the pore size distribution curves. The NMR fractal dimension D_{meso} and N_2 adsorption fractal dimension D_2 are both related to the mesopore, which explains the strong positive relationships between them (Fig. 10b). The NMR relaxation process of micropore is related to the hydrogen nuclei of the pore surface, different from the that of mesopore which is related to the pore size (Zhang et al., 2003). If the pores have larger surface area or rougher surface, there are more hydrogen nuclei on the pore surface, the relaxation signal becomes stronger, and there are more micropore. It means that the NMR fractal dimension D_{micro} mainly reflects the surface complexity of pore surface, and this is identical with the definition of the N_2 adsorption fractal dimension D_1 as mentioned in Section 4.5. This leads to the strong positive relationship between these two fractal dimensions (Fig. 10a).

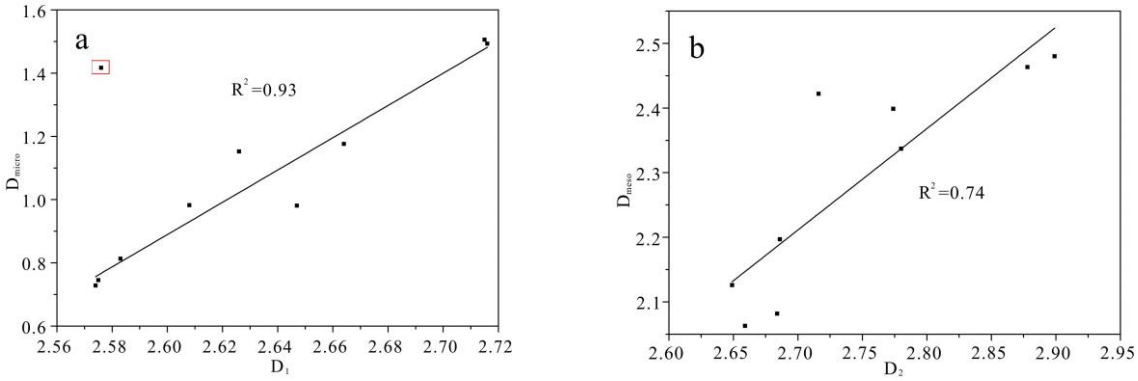

Fig. 10. Relationships between D_{micro} and D_1 (a), D_{meso} and D_2 (b).

5.5 Effects of mineralogical composition, pore structure and fractal dimension on surface relaxivity

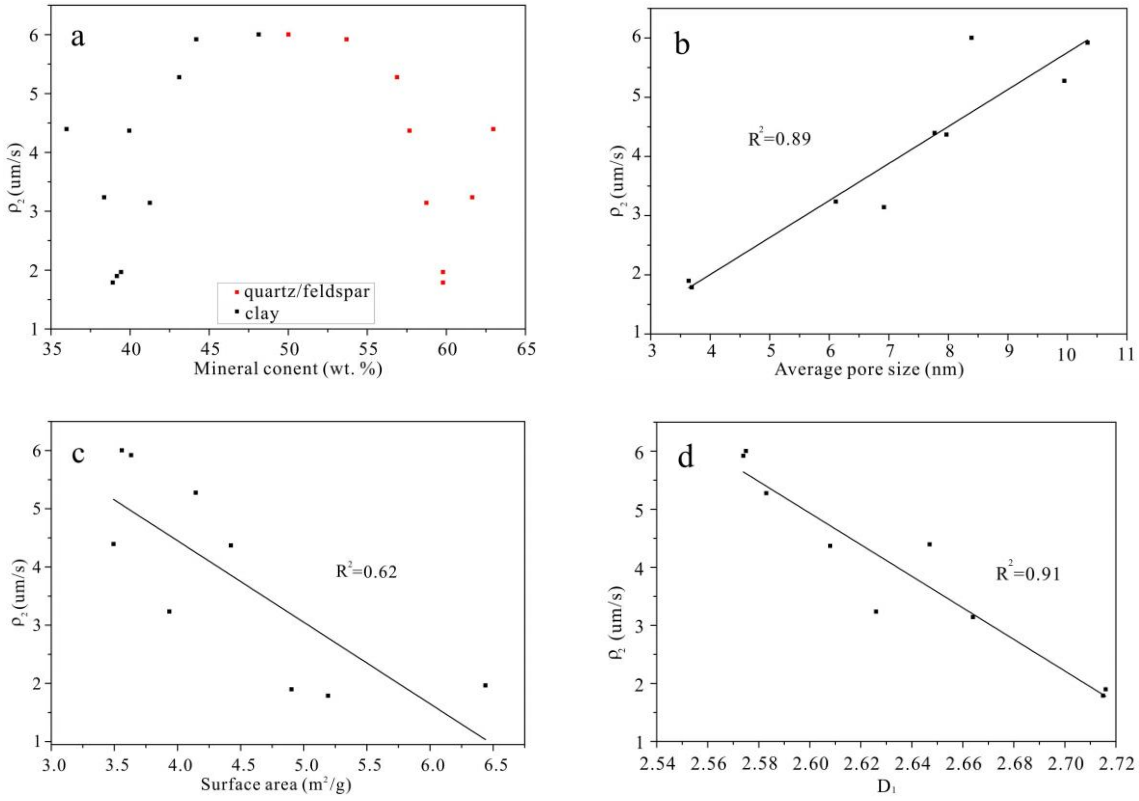

Fig. 11. Relationships between surface relaxivity and mineral content (a), average pore size (b), surface area (c) and D_1 (d).

From Fig. 11a, it can be seen that the shale samples with rich quartz/feldspar have a higher surface relaxivity, while the samples with rich clay minerals have a lower surface relaxivity. Fleury calculated the surface relaxivity of sandstone, ranging from 3.5um/s to 11.7 um/s, with an average value of 6.48 um/s (Fleury, 2007), which is higher than the average value of the studied shale samples, i.e. 3.8 um/s. Chang found that the surface relaxivity of carbonates was smaller than that of quartz (Chang et al., 1994). Saidian found that the surface relaxivity has a strong positive relationship with the content of illite (Saidian and Prasad, 2015). Thus, it can be inferred that the surface relaxivity is related to mineralogical composition (Coates et al., 1999). Surface relaxation is the result of fluid-solid interaction in porous media and can be quantitatively evaluated by surface relaxivity (Saidian and Prasad, 2015). In addition to the influence of the mineralogical composition, the surface relaxivity is also related to the pore size and the pore surface (Coates et al., 1999). As the surface area of porous media gets larger, more spinning hydrogen nuclei get involved, and the relaxation rate becomes larger (Chu et al., 2007). Fig. 11b-c shows that the shale surface relaxivity has a strong positive relationship and a strong negative relationship with the average pore size and surface area respectively, and the R^2 is 0.89 and 0.62 respectively. It indicates that as the average pore size gets smaller and the surface area gets larger, despite that more spinning hydrogen nuclei will be involved in the relaxation, causing the relaxation rate increasing, the corresponding surface relaxivity gets smaller. The N_2 fractal dimension D_1 reflects the fractal characteristics of the pore surface. If D_1 gets larger, the pore surface becomes more irregular and rougher, and more spinning hydrogen nuclei can be involved in relaxation. The strong negative relationship between the surface relaxivity and D_1 (Fig. 11d) shows that as the fractal dimension D_1 gets larger, the pore surface becomes rougher and the surface relaxivity becomes smaller.

6 Conclusions

In this paper, we investigated the full-sized pore structure and fractal characteristics of the Marine-Continental transitional shale of lower Permian in Qinshui Basin using a variety of measurements and fractal theory. The following conclusions can be made:

(1) The TOC content of the Marine-Continental transitional shale of the lower Permian in Qinshui Basin is relatively high, with an average value of 2.44% (wt.), and the thermal evolution is during the mature-over mature stage. The mineralogical composition is mainly clay minerals which are primarily composed of I/S, followed by kaolinite, illite and chlorite.

(2) The NMR T_2 spectrum can characterize the full-sized pore structure characteristics of shale. The statistics show that the pore volume is mainly provided by mesopore, followed by micropore; the surface area is mainly provided by micropore, followed by mesopore; macropore contributes little to pore volume and surface area.

(3) The pore volume and surface area of shale in Qinshui Basin are controlled by clay minerals and have no relationships with TOC. The kaolinite and I/S control the pore structure characteristics of micropore and mesopore-macropore respectively.

(4) The NMR fractal dimensions D_{micro} can be used to characterize the fractal characteristics of pore surface, and D_{meso} can be used to characterize the fractal characteristics of pore structure.

(5) The surface relaxivity $\rho 2$ is controlled by mineralogical composition, pore structure and fractal characteristics. The higher clay mineral content, smaller average pore size, larger surface area or larger fractal dimension of pore surface will all result in a smaller surface relaxivity.

Acknowledges

This study received support from the National Science and Technology Major Project of China (Grant No. 2016ZX05034). We would like to thank anonymous reviewers for their comments and suggestions

References

Barrett E.P., Joyner L.G., and Halenda P.P., 1951. The determination of pore volume and area distributions in porous substances. I. Computations from nitrogen isotherms. *Journal of the American Chemical Society*. 73 (1), 373－380.

Benavides F., Leiderman R., Souza A., Carneiro G., and Bagueira R., 2017. Estimating the surface relaxivity as a function of pore size from NMR T2 distributions and micro-tomographic images. *Computer & Geosciences*. 106 200－208.

Bernal J., and Bello M.A., 2001. Fractal geometry and mercury porosimetry - Comparison and application of proposed models on building stones. *Applied Surface Science*. 185 (1-2), 99－107.

Brunauer S., Emmett P.H., and Teller E., 1938. Adsorption of gases in multimolecular layers. *Journal of the American Chemical Society*. 60 (2), 309－319.

Cai J., Luo L., Ye R., Zeng X., and Hu X., 2015. Recent advances on fractal modeling of permeability for fibrous porous media. *Fractals*. 23 (1), 1－9.

Cai Y.D., Liu D.M., Pan Z.J., Yao Y.B., Li J.Q., and Qiu Y.K., 2013. Pore structure and its impact on CH4 adsorption capacity and flow capability of bituminous and subbituminous coals from Northeast China. *Fuel*. 103 258－268.

Chalmers G.R., Bustin R.M., and Power I.M., 2012. Characterization of gas shale pore systems by porosimetry, pycnometry, surface area, and field emission scanning electron microscopy/transmission electron microscopy image analyses: Examples from the Barnett, Woodford, Haynesville, Marcellus, and Doig units. *AAPG Bulletin*. 96 (6), 1099－1119.

Chang D., Vinegar H., Morriss C., and Straley C., 1994. Effective porosity, producible fluid, and permeability in carbonates

from NMR logging. *Log Analyst*. 38 (2), 60－72.
Chen L., Jiang Z.X., Liu K.Y., Gao F.L., and Wang P.F., 2017. A combination of n-2 and CO2 adsorption to characterize nanopore structure of Organic-Rich lower silurian shale in the upper yangtze platform, south china: Implications for shale gas sorption capacity. *Acta Geologica Sinica* (English Edition). 91 (4), 1380－1394.
Chu Z.H., Gao J., Huang L.J., and Xiao L.Z., 2007. Geophysical well logging methods and principles. Beijing, Petroleum Industry Press.
Clarkson C.R., Solano N., Bustin R.M., Bustin A.M.M., Chalmers G.R.L., He L., Melnichenko Y.B., Radlinski A.P., and Blach T.P., 2013. Pore structure characterization of North American shale gas reservoirs using USANS/SANS, gas adsorption, and mercury intrusion. *Fuel*. 103 (A), 606－616.
Coates G.R., Xiao L.Z., and Prammer M.G., 1999. NMR logging principles and applications. Houston(Texas), Gulf Professional Publishing.
Curtis J.B., 2002. Fractured shale-gas systems. *AAPG Bulletin*. 86 (11), 1921－1938.
Curtis M.E., Cardott B.J., Sondergeld C.H., and Rai C.S., 2012. Development of organic porosity in the Woodford Shale with increasing thermal maturity. *International Journal of Coal Geology*. 102 26－31.
Dollimore D., Heal G.R., 1964. An improved method for the calculation of pore size distribution from adsorption data. *Journal of Chemical Technology & Biotechnology Biotechnology*. 14 (3), 109－114.
Fleury M., 2007. NMR surface relaxivity determination using NMR apparent diffusion curves and BET measurements. In: *International Symposium of the Society of Core Analysts*. Calgary, Canada.
Fu H.J., Tang D.Z., Xu T., Xu H., Tao S., Li S., Yin Z.Y., Chen B.L., Zhang C., and Wang L.L., 2017. Characteristics of pore structure and fractal dimension of low-rank coal: A case study of Lower Jurassic Xishanyao coal in the southern Junggar Basin, NW China. *Fuel*. 193 254－264.
Fu J., Guo S., Gao Q., and Yang J., 2016. Reservoir characteristics and enrichment conditions of shale gas in the Carboniferous-Permian coal-bearing formations of Qinshui Basin. *Earth Science Frontiers* (in Chinese with English abstract). 23 (2), 167－175 .
Gong X., Tang H., Zhao F., Wang J., and Xiong H., 2016. Quantitative characterization of pore structure in shale reservoir of Longmaxi Formation in Sichuan Basin. *Lithologic Reservoirs* (in Chinese with English abstract). 28 (3), 48－57.
Han H., Liu P.W., Ding Z.G., Shi P.T., Jia J.C., Zhang W., Liu Y., Chen S.J., Lu J.G., Chen K., Peng X.D., Wang Z.Y., Xiao S.Q., and Gao Y., 2018. The influence of extractable organic matter on pore development in the late triassic chang 7 lacustrine shales, yanchang formation, ordos basin, china. *Acta Geologica Sinica* (English Edition). 92 (4), 1508－1522.
Horváth G., and Kawazoe K., 1983. Method for the calculation of effective pore size distribution in molecular sieve carbon. *Journal of Chemical Engineering of Japan*. 16 (6), 470－475.
Ji L., Qiu J., and Xia Y., 2012. Micro-pore characteristics and methane adsorption properties of common clay minerals by electron microscope scanning. *Acta Petrolei Sinica* (in Chinese with English abstract). 33 (2), 249－256.
Jiang Z., Tang X., Li Z., Huang H., Yang P., Yang X., Li W., and Hao J., 2016. The whole-aperture pore structure characteristics and its effect on gas content of the Longmaxi Formation shale in the southeastern Sichuan basin. *Earth Science Frontiers* (in Chinese with English abstract). 23 (2), 126－134.
Kuila U., and Prasad M., 2013. Specific surface area and pore-size distribution in clays and shales. *Geophysical Prospecting*. 61 (2SI), 341－362.
Labani M.M., Rezaee R., Saeedi A., and Al Hinai A., 2013. Evaluation of pore size spectrum of gas shale reservoirs using low pressure nitrogen adsorption, gas expansion and mercury porosimetry: A case study from the Perth and Canning Basins, Western Australia. *Journal of Petroleum Science and Engineering*. 112 7－16.
Li A., Ding W., Jiu K., Wang Z., Wang R., and He J., 2018. Investigation of the pore structures and fractal characteristics of marine shale reservoirs using NMR experiments and image analyses: A case study of the Lower Cambrian Niutitang Formation in northern Guizhou Province, South China. *Marine and Petroleum Geology*. 89 (3), 530－540.
Li X., Li Q., and Dong L., 2014. On impact of paramagnetic substances on nuclear magnetic porosity of intermediate to basic volcanic rocks. *Well Logging Technology* (in Chinese with English abstract). 38 (5), 522－525.
Liang J., Zhu X., Liu Y., Wang C., and Lu Y., 2016. Comparative study on accumulation conditions of the tight gas in the upper paleozoic of the Qinshui Basin and Ordos Basin and its exploration potential. *Journal of China Coal Society* (in Chinese). 41 (1), 192－201.
Liang J., Wang C., Liu Y., Gao Y., Du Jiangfeng, Feng R., Zhu X., and Yu J., 2014. Study on the tight gas accumulation conditions・and exploration potential in the qinshui basin. *Natural Gas Geoscience* (in Chinese). 25 (10), 1509－1519.
Loucks R.G., Reed R.M., Ruppel S.C., and Jarvie D.M., 2009. Morphology, genesis, and distribution of nanometer-scale pores in siliceous mudstones of the mississippian barnett shale. *Journal of Sedimentary Research*. 79 (11－12), 848－861.
Loucks R.G., Reed R.M., Ruppel S.C., and Hammes U., 2012. Spectrum of pore types and networks in mudrocks and a descriptive classification for matrix-related mudrock pores. *AAPG Bulletin*. 96 (6), 1071－1098.
Ning Y.X., Jiang Z.X., Su S.Y., Li T.W., Chen W.T., Chen L., and Wang Z., 2016. Method of calculating pore radius distribution in shale reservoirs from NMR T-2 spectra. *Science Technology and Engineering* (in Chinese). 16 (27), 14－19.
Pfeifer P., and Avnir D., 1983. Chemistry nonintegral dimension between two and three. *Chemical Physics*. 79 (7), 3369－3558.
Pyun S.I., and Rhee C.K., 2004. An investigation of fractal characteristics of mesoporous carbon electrodes with various pore structures. *Electrochemica Acta*. 49 (24), 4171－4180.
Quantachrome. Autosorb AS-1/ASWin gas sorption system operation manual. Boynton Beach, Florida: Quantachrome Instruments; 2008. p.
Rand B., 1976. On the empirical nature of the Dubinin—Radushkevich equation of adsorption. *Journal of Colloid & Interface Science*. 56 (2), 337－346.
Ravikovitch P.I., and Neimark A.V., 2006. Density functional theory model of adsorption on amorphous and microporous silica materials. *Langmuir*. 22 (26), 11171－9.
Ross D.J.K., and Bustin R.M., 2009. The importance of shale composition and pore structure upon gas storage potential of shale gas reservoirs. *Marine and Petroleum Geology*. 26 (6), 916－927.
Saidian M., and Prasad M., 2015. Effect of mineralogy on nuclear magnetic resonance surface relaxivity: A case study of Middle Bakken and Three Forks formations. *Fuel*. 161 197－206.
Saidian M., Kuila U., Saul R., Godinez L.J., and Prasad M., 2014. Porosity and pore size distribution in mudrocks: A comparative study for haynesville, niobrara, monterey and eastern european silurian formations. In: *Unconventional Rsrources Technology Conference*. Denver, Colorado, USA.
Sing K., Evereft D.H., Haul R., Moscou L., Pierottira R.A., Rouquerol J., and Siemieniewska T., 1985. Reporting physisorption data for Gas/Solid systems with specil reference to the determination of surface area and porosity. *Pure and Applied Chemistry*. 57 (4), 603－619.

STRALEY C., VINEGAR H., and MORRISS C., 1997. Core analysis by low field NMR. *Log Analyst*. 38 (2), 43－56.
Wang P., Jiang Z., Ji W., Zhang C., Yuan Y., Chen L., and Yin L., 2016. Heterogeneity of intergranular, intraparticle and organic pores in Longmaxi shale in Sichuan Basin, South China: Evidence from SEM digital images and fractal and multifractal geometries. *Marine and Petroleum Geology*. 72 122－138.
Wang Y., Zhu Y., Liu S., and Zhang R., 2016. Pore characterization and its impact on methane adsorption capacity for organic-rich marine shales. *Fuel*. 181 227－237.
Xi Z., Tang S., Li J., and Li L., 2017. Investigation of pore structure and fractal characteristics of marine-continentaltransitional shale in the east-central of Qinshui Basin. *Natural Gas Geoscience*. 28 (3), 366－376 (in Chinese).
Xiong F.Y., Jiang Z.X., Li P., Wang X.Z., Bi H., Li Y.R., Wang Z.Y., Amooie M.A., and Soltanian M.R., Moortgat J., 2017. Pore structure of transitional shales in the Ordos Basin, NW China: Effects of composition on gas storage capacity. *Fuel*. 206 504－515.
Yan Y.B., and Liu D.M., 2016. Petrophysics and fluid properties characterization of coalbed methane reservoir by using NMR relaxation time analysis. *Coal Science and Technology* (in Chinese with English abstract). 44 (06), 14－22.
Yang C., Zhang J.C., Wang X.Z., Tang X., Chen Y.C., Jiang L.L., and Gong X., 2017. Nanoscale pore structure and fractal characteristics of a marine-continental transitional shale: A case study from the lower Permian Shanxi Shale in the southeastern Ordos Basin, China. *Marine and Peteoleum Geology*. 88 54－68.
Yang C., Zhang J., Tang X., Ding J., Zhao Q., Dang W., Chen H., Su Y., Li B., and Lu D., 2017. Comparative study on micro-pore structure of marine, terrestrial, and transitional shales in key areas, China. *International Journal of Coal Geolgy*. 171 76－92.
Yang F., Ning Z.F., and Liu H.Q., 2014. Fractal characteristics of shales from a shale gas reservoir in the Sichuan Basin, China. *Fuel*. 115 378－384.
Yang K., Lu X., Liu X., and Hou Q., 2006. Characterization technique ii of mineral material based on probe gas adsorption isotherm:nano-pore structure of porous material. *Bulletin of mineralogy petrology and geochemistry* (in Chinese). 25 (4), 362－368.
Yao Y., Liu D., Tang D., Tang S., and Huang W., 2008. Fractal characterization of adsorption-pores of coals from North China: An investigation on CH4 adsorption capacity of coals. *International Journal of Coal Geolgoy*. 73 (1), 27－42.
Yao Y.B., Liu D.M., Che Y., Tang D.Z., Tang S.H., and Huang W.H., 2010. Petrophysical characterization of coals by low-field nuclear magnetic resonance (NMR). *Fuel*. 89 (7), 1371－1380.
Yu B., 2013. Classification and characterization of gas shale pore system. *Earth Science Frontiers* (in Chinese). 20 (04), 211－220.
Zhang G.Q., Hirasaki G.J., and House W.V., 2003. Internal field gradients in porous media. *Petrophysics*. 44 (6), 422－434.
Zhang J., Li X., Wei Q., Sun K., Zhang G., and Wang F., 2017. Characterization of Full-Sized pore structure and fractal characteristics of Marine-Continental transitional longtan formation shale of sichuan basin, south china. *Energy & Fuels*. 31 (10), 10490－10504.
Zhang Y.S., Zheng M.P., Xing E.Y., Li Y.C., Gui B.L., Shi L.Z., He Y.T., Wang L.L., Peng Y., and Zhao H.T., 2017. Discovery of Marine-terrestrial Transitional Facies Shale Gas in Taiyuan Formation of Zhenjia 1 Well, Northern Shaanxi, Ordos basin. *Acta Geologica Sinica* (English Edition). 91 (3), 1141－1142.
Zhang Z., and Weller A., 2014. Fractal dimension of pore-space geometry of an Eocene sandstone formation. *Geophysics*. 79 (6), D377－D387.
Zhou L., and Kang Z., 2016. Fractal characterization of pores in shales using NMR: A case study from the Lower Cambrian Niutitang Formation in the Middle Yangtze Platform, Southwest China. *Journal of Natural Gas Science and Engineering*. 35 (A), 860－872.
Zhou S., Liu D., Cai Y., and Yao Y., 2016. Fractal characterization of pore-fracture in low-rank coals using a low-field NMR relaxation method. *Fuel*. 181 218－226.
Zou C., Zhu R., Bai B., Yang Z., Wu S., Su L., and Dong D., Li X., 2011. First discovery of nano-pore throat in oil and gas reservoir in China and its scientific value. *Acta Petroleum Sinica* (in Chinese). 27 (6), 1857－1864.
Zuo Z., Zhang X., Chen S., Si Q., Zhang C., and Liu Z., 2017. Heterogeneity of shale gas reservoirs in coal measures: A case study of the taiyuan and shanxi formations in the ningwu basin. *Acta Geologica Sinic*a. 91 (5), 1130－1140.

About the first author

Yin Liangliang, male, born in 1988 in Nanyang City, Henan Province; a Ph.D. student of School of Energy Resources at China University of Geosciences (Beijing). His research focuses on reservoir evaluation of unconventional oil and gas. E-mail: yllybyq@126.com.

About the corresponding author

Guo Shaobin, male, born in 1963 in Shandong Province; post doctorate, graduated from China University of Geosciences (Beijing); professor of School of Energy Resources at China University of Geosciences (Beijing). His research focuses on reservoir prediction and evaluation. His more recent work is on occurrence mechanism and accumulation regularity of marine-continental transitional shale gas. E-mail: guosb58@126.com.